Journal of Sound and Vibration 470 (2020) 115157

Contents lists available at ScienceDirect

Journal of Sound and Vibration

journal homepage: www.elsevier.com/locate/jsvi

A spectral pedestrian-based approach for modal identification

André Jesus [a,*], Stana Živanović [b], Amir Alani [c]

[a] Faculty of Environment and Technology, University of the West of England, Coldharbour Lane, Frenchay Campus, Bristol, BS16 1QY, UK
[b] College of Engineering, Mathematics and Physical Sciences, University of Exeter, Exeter, EX4 4QF, UK
[c] School of Computing and Engineering, University of West London, St. Mary's Road, Ealing, London, W5 5RF, UK

ARTICLE INFO

Article history:
Received 29 April 2019
Revised 11 December 2019
Accepted 13 December 2019
Available online 19 December 2019
Handling Editor: J. Macdonald

Keywords:
Power spectral density
Modal identification
FRP footbridge
Pedestrian excitation
Metropolis–Hastings
Likelihood function

ABSTRACT

The dynamic behaviour of footbridges is characterised by modal properties such as natural frequencies, mode shapes, damping ratios and modal masses. Their estimation via modal tests often requires expensive or difficult-to-operate equipment (e.g. shaker and instrumented impact hammer) or, sometimes unavailable high signal-to-noise ratios in tests relying on natural (e.g. wind, airborne noise and ground-borne vibration) excitation. In addition, the modal properties determined in modal tests do not necessarily apply to the structure under pedestrian traffic in case of amplitude-dependent frequencies and damping ratios. The current work proposes a novel approach that stands in contrast to the widely used tests, based on modal identification using an excitation induced by a single pedestrian. In order to account for estimation and observation uncertainties, the relationship between the power spectrum of the response and its modal properties is described with a likelihood function. It is shown that it is possible to reliably estimate modal properties using pedestrian walk forces measured in the laboratory, and dynamic responses measured when the same pedestrian is crossing a footbridge at timed pacing rates. The approach is validated using numerical and field data for a 16.9 m long fibre reinforced polymer footbridge. This work paves a new way for simple and low cost modal testing in structural dynamics.

1. Introduction

Structural assessment via modal testing is a vast area of research, enabled by advanced signal processing techniques and excitation methods [1]. The selected approach is often based on operational constraints, such as time, cost-effectiveness, ease-of-use, type of structure and available excitation.

Flexible large-scale structures are usually best tested using ambient excitation. Data analysis employs methods that are developed assuming that vibrations are random (i.e. broadband) and that signal-to-noise ratio (SNR) is high. Much progress has been made in the processing techniques that utilise these types of measurements [2–5]. For medium-scale structures, the most significant modes of vibration might be excitable with more controllable sources: such as instrumented moving vehicles [6], or with medium/high-force shakers. Finally for structures such as footbridges, the main equipment for excitation are portable shakers and hand-held impact hammers, although ambient testing is occasionally used as well.

Both shakers and impact hammers have their drawbacks. With a shaker, the frequency response function (FRF) is constructed from the excitation signal (such as sweep sine, chirp, or random excitation) and simultaneously measured vibration responses.

* Corresponding author.
E-mail address: andrehjesus@gmail.com (A. Jesus).

https://doi.org/10.1016/j.jsv.2019.115157

This type of test is very reliable, but it is expensive and might be difficult to execute in difficult-to-access sites due to heavy weight of the shaker (often more than 50 kg). Hammer impact testing drawbacks are poor SNR, high sensitivity to non-linearities and a lack of control over the frequency content of the excitation. Concerning cost-effectiveness of these two solutions, the impact hammer provides the more economic option, that could be about ten times less expensive than testing with the shaker [7]. Ambient test is similarly affordable, but could suffer from low SNR.

In all these tests the identification of natural frequencies is the most reliable and modal masses are the most difficult (or even impossible in the ambient testing) to identify. It is not uncommon to see errors in the order of 1% for natural frequencies and 30% for damping ratios and modal masses—as illustrated in Section 18.5.3 of [8] and Chapter 1 of [9]. As a consequence, some have instead tried to estimate modal masses with human tests, as proposed by Brownjohn and Pavic [10]. Such tests are attractive since they are cost-effective, easy and quick to perform. In addition, Brownjohn and his co-workers [11] used human excitation generated whilst jumping and measured using either a force plate or inertial measurement units. They also measured acceleration response of the structure to estimate the frequency response function (FRF) of one vibration mode at a time. It should be noted that nearly all examples of this body of research relied solely on jumping tests to identify properties of individual vibration modes. Probabilistic models were seldom used despite of the inherent uncertainties [12–14].

This work investigates the applicability of a modal identification approach using the dynamic excitation by a pedestrian. In contrast to the previous research, the proposed approach can be used for simultaneous identification of multiple vibration modes, and it accounts for estimation and observation uncertainties using a likelihood function of the "bridge-pedestrian" spectral response. The identification process requires two main inputs: recordings at a range of pacing rates of structural responses under passage of a given pedestrian; and the pedestrian-induced dynamic forces (measured on, say, an instrumented treadmill in a laboratory at the same pacing rates). Validation is illustrated with both simulated and field data from a 16.9 m long fibre reinforced polymer (FRP) footbridge, for which results of modal analysis are available [15,16].

The introduction section is followed by Section 2 that presents the footbridge case-study for validation of the proposed approach. Section 3 details how the structural system is modelled and how it connects the input excitation to the output response. Section 4 further details the human-input excitation. Section 5 provides the linkage of this model with measured data, through a statistical framework that identifies the target modal properties. Sections 6 and 7 highlight the main results/discussion and conclusions of this work, respectively.

2. Case-study footbridge

This section presents a case-study FRP footbridge and a summary of testing carried out to infer its dynamic properties. All modal properties, except modal masses, were estimated using the instrumented hammer modal testing technique and free-decay measurements [15], whilst the modal masses were obtained from an FE model [16]. These properties will be used as a validation metric for the approach developed in this work.

2.1. General

The footbridge under analysis is a 16.9 m single span beam structure that crosses a river valley (Fig. 1a). Pultruded fibre-reinforced polymer panels interlock to form a square 0.78 m wide cross-section (Fig. 1b). The bridge's total mass is approximately 1800 kg. Further details relating to the bridge can be found elsewhere [15].

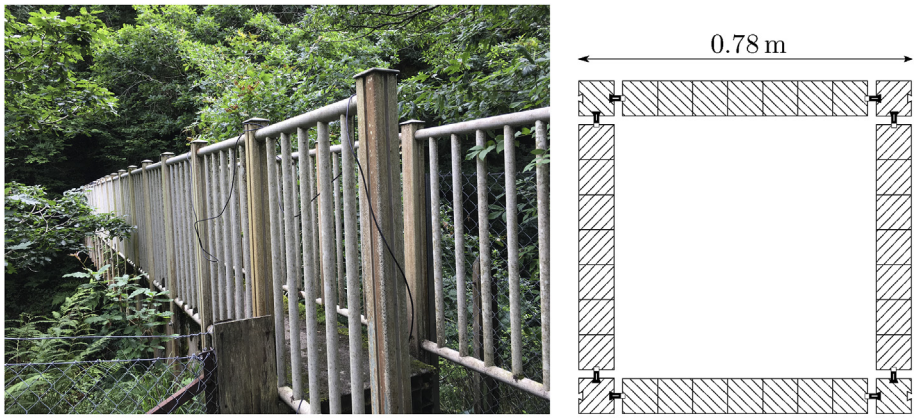

Fig. 1. Lively footbridge (a) general view and (b) cross section of individual units that form the footbridge deck.

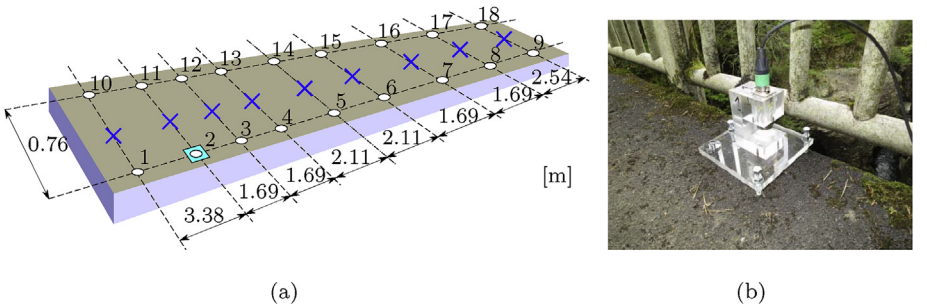

Fig. 2. Impact hammer testing (a) measurement grid with circles and square representing response and hammer impact points, respectively, and (b) accelerometer on footbridge deck.

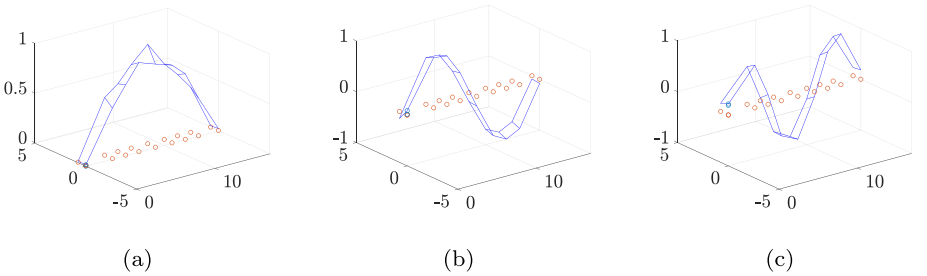

Fig. 3. Unity normalised (a) first (b) second and (c) third vertical mode shapes.

2.2. Modal testing

The current section summarises details about modal tests on the footbridge. A detailed description of modal tests can be found in Ref. [15] and of FE analysis in Ref. [16]. A modal test using an impact hammer was carried out to identify vertical flexural and/or torsional vibration modes in the frequency range up to 30 Hz. Additionally, the structure was excited by a pedestrian walking at metronome controlled pacing rates from 1.40 Hz to 2.45 Hz in increments of 0.10 Hz or 0.05 Hz – depending of the pacing rate's proximity to identified natural frequencies. To check repeatability two walks were recorded for each pacing rate. The vibration response was measured at two locations on the deck, and it included recording of the free decay in the response after each crossing.

A measurement grid of 18 points (Fig. 2a) was used to determine the modal properties. Three roving accelerometers, one of which is shown in Fig. 2b (model QA750 by Honeywell, nominal sensitivity of 1300 mVg^{-1}), were used to simultaneously measure response to hammer impact applied at test point 2 (TP2). After completing one set of measurements at three TPs, the accelerometers were moved to the next there points until the whole grid of 18 TPs was covered, as in a typical roving tri-axial accelerometer test [17].

Impact was applied manually by an experienced operator using an instrumented sledgehammer (model 5803A by Dytran, nominal sensitivity 0.23 mVN^{-1} and measurement range of 22.2 kN). Data were sampled at 512 Hz. For the walk tests, vertical responses were measured only at TP2 and TP5 at a sampling rate of 256 Hz. All signals were acquired using a 24-bit, four channel Quattro (by Data Physics) data logger and analyser.

The accelerance FRFs were calculated using six averages. Three flexural vertical modes of vibration at about 4.8 Hz, 15.1 Hz and 28.9 Hz have been identified and their unity-normalised mode shapes are shown in Fig. 3. By analysing free decay measurements, it was found that the natural frequency and damping ratio for the fundamental mode are amplitude-dependent, with frequency decreasing from 4.87 Hz to 4.57 Hz and damping ratio increasing from 2.05% to 2.45% when vibration amplitude increases up to 1.5 ms^{-2} [15]. The natural frequencies and damping ratios for the three modes are shown in Table 1. Finally, due to poor repeatability, the modal masses could not be estimated from the experimental data. This is frequently the case in modal testing, which is the reason why modal mass information is rarely reported in literature. To overcome this situation an FE model of the bridge has been developed, and it is described in detail in Ref. [16]. The estimated frequencies were 4.9 Hz, 15.8 Hz and 31.4 Hz, and were judged to be sufficiently close to those measured (for estimation of the modal masses) so not to perform further FE model updating. The resulting modal masses were found to be 862 kg, 907 kg and 839 kg, respectively.

Table 1
Modal properties identified in impact hammer and free decay tests.

f_1	f_2	f_3 (Hz)	ζ_1	ζ_2	ζ_3 (%)
4.57–4.87	15.1	28.9	2.05–2.45	2.8	2.7

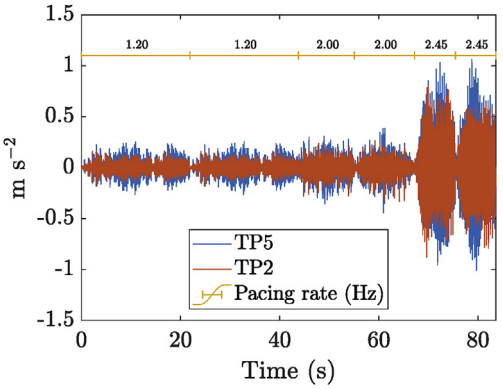

Fig. 4. Acceleration responses of footbridge at TP2 and TP5 for three pacing rates at 1.20 Hz, 2.00 Hz and 2.45 Hz.

Sample acceleration responses to walking at 1.20 Hz, 2.00 Hz and 2.45 Hz are displayed in Fig. 4.
These results constitute the main validation data for the pedestrian-based approach presented next.

3. Theoretical framework

The pedestrian-based approach is detailed in the following sections and is illustrated in Fig. 5. The core idea is to match power spectral densities (PSD) of responses induced by a pedestrian on the bridge against theoretical PSDs. The latter are based on forces obtained using a laboratory treadmill [24] and a probabilistic model of the structure. For the current work there is an eight years gap between in-field and treadmill experiments. Although this is a significant period of time, the test subject is well experienced in walking tests, has body mass which hardly changed over time, and has been generating very much the same peak responses when walking over structures similar to the one presented.

The to-be-identified modal properties – natural frequencies, damping ratios and modal masses – are denoted as θ. The framework was implemented with MATLAB.

3.1. Equation of motion – time domain

The general equation of motion of a structural system with N_d DOFs can be written as follows

$$\mathbf{M}\ddot{\mathbf{y}}(t) + \mathbf{C}\dot{\mathbf{y}}(t) + \mathbf{K}\mathbf{y}(t) = \mathbf{x}(t) \tag{1}$$

for a scenario of damped forced vibrations. $\mathbf{M}$, $\mathbf{C}$ and $\mathbf{K}$ are $N_d \times N_d$ mass, damping and stiffness matrices, $\ddot{\mathbf{y}}$, $\dot{\mathbf{y}}$, $\mathbf{y}$ and $\mathbf{x}$ are $N_d \times 1$ time-dependent vectors of acceleration, velocity, displacement and force induced by a pedestrian at each DOF, respectively. Commonly this equation is transformed into its modal equivalent by using the transformation $\mathbf{y}(t)_{N_d \times 1} = \mathbf{\Phi}_{N_d \times n}\, \mathbf{q}(t)_{n \times 1}$ (for n independent vibration modes), with $\mathbf{\Phi} = [\mathbf{\Phi}_1 \mathbf{\Phi}_2 \dots \mathbf{\Phi}_n]$ defined as an $N_d \times n$ mode shape matrix. Pre-multiplying Eq. (1) by the transposed mode shape matrix $\mathbf{\Phi}^{\mathrm{T}}$ results in

$$\mathbf{m}\ddot{\mathbf{q}}(t) + 2\mathbf{m}\boldsymbol{\zeta}\boldsymbol{\omega}_n\dot{\mathbf{q}}(t) + \mathbf{m}\boldsymbol{\omega}_n^2\mathbf{q}(t) = \mathbf{\Phi}^{\mathrm{T}}(t)\mathbf{x}(t) \tag{2}$$

where $\mathbf{m}$, $\boldsymbol{\zeta}$, $\boldsymbol{\omega}_n$ are the n-dimensional diagonal matrices that contain the modal masses, damping ratios and circular natural frequencies, respectively. The vector on the right-hand side represents time-dependent modal forces for given modes, and $\mathbf{q}$, $\dot{\mathbf{q}}$, $\ddot{\mathbf{q}}$ are the modal response vectors of displacement, velocity and acceleration, respectively. It should be noted that the mode shape matrix on the RHS of Eq. (2) can be transformed from spatial to time domain using $t = l/v$, where l is the longitudinal position of the pedestrian on the bridge while v is the pedestrian speed (assumed to be constant).

3.2. Frequency response function – frequency domain

In this section Eq. (1) is analysed in the frequency domain with the aid of the Fourier transform (FT). Taking Eq. (2) as a basis, and applying the FT to convert it from time into frequency domain, results in

$$\mathbf{m}\ddot{\mathbf{Q}}(\omega) + 2\mathbf{m}\boldsymbol{\zeta}\boldsymbol{\omega}_n\dot{\mathbf{Q}}(\omega) + \mathbf{m}\boldsymbol{\omega}_n^2\mathbf{Q}(\omega) = \overline{\mathbf{X}}(\omega) \tag{3}$$

where $\ddot{\mathbf{Q}}$, $\dot{\mathbf{Q}}$, $\mathbf{Q}$ and $\overline{\mathbf{X}}$ represent the FTs of the modal responses and modal forces, respectively. In the present work the complex form of the FT is defined as

$$X(\omega) = \frac{1}{2\pi}\int_{-\infty}^{\infty} x(t)\mathrm{e}^{-\mathrm{i}\omega t}dt. \tag{4}$$

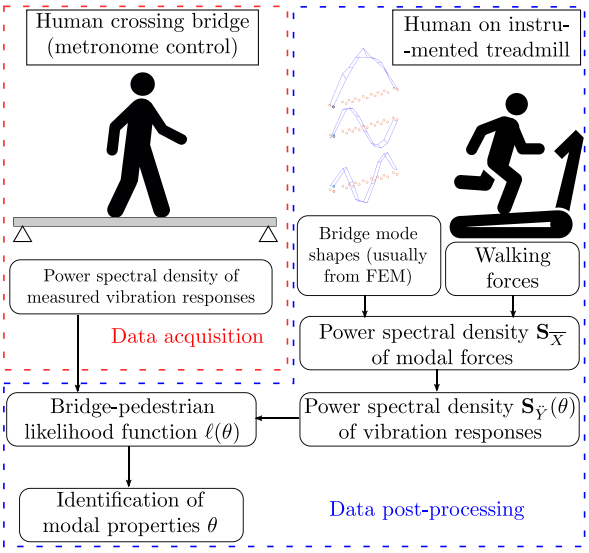

Fig. 5. Diagram of spectral pedestrain-based approach.

By definition $\ddot{\mathbf{Q}} = -\omega^2\mathbf{Q}$, $\dot{\mathbf{Q}} = \mathrm{i}\omega\mathbf{Q}$ and $\ddot{\mathbf{Q}} = \mathrm{i}\omega\dot{\mathbf{Q}}$. The FT of the modal acceleration response can be written as:

$$\ddot{\mathbf{Q}}(\omega) = \mathbf{H}(\omega)\overline{\mathbf{X}}(\omega). \tag{5}$$

where $\mathbf{H}$ is an n-dimensional diagonal FRF matrix, which is a function of the structural modal properties. Accelerance FRF for a single degree of freedom system is given by

$$H(\omega) = \frac{-\omega^2}{m(-\omega^2 + \omega_n^2 + 2\zeta\mathrm{i}\omega_n\omega)}. \tag{6}$$

Now the FT of physical acceleration can be written as

$$\ddot{\mathbf{Y}}(\omega)_{N_d\times 1} = \mathbf{\Phi}_{N_d\times n}\ddot{\mathbf{Q}}(\omega)_{n\times 1} = \mathbf{\Phi}_{N_d\times n}\mathbf{H}(\omega)_{n\times n}\overline{\mathbf{X}}(\omega)_{n\times 1}. \tag{7}$$

Assuming that the response has random fluctuations in it, an N_d-dimensional Hermitian PSD matrix at frequency ω can be obtained from the FT of the response in Eq. (7) as follows

$$\mathbf{S}_{\ddot{\mathbf{y}}}(\omega) = \mathrm{E}[\ddot{\mathbf{Y}}(\omega)\ddot{\mathbf{Y}}(\omega)^{\mathrm{H}}] = \mathbf{\Phi}_{N_d\times n}\,\mathbf{H}(\omega)_{n\times n}\,\mathbf{S}_{\overline{X}}(\omega)^{n\times n}\mathbf{H}(\omega)^{\mathrm{H}}_{n\times n}\mathbf{\Phi}^{\mathrm{T}}_{n\times N_d}, \tag{8}$$

where $\mathbf{S}_{\overline{X}}$ is an n-dimensional Hermitian PSD matrix of modal forces. This matrix contains in its diagonal and off-diagonal entries the auto and cross PSD between modal forces, respectively. Eq. (8) is the central result of random vibration theory for a multiple DOF system, and it will be utilised as a data model of the bridge-pedestrian system which allows to estimate modal properties.

4. Spectral model of the excitation

This section details how the PSD matrix of modal forces in Eq. (8) is obtained. The following text adopts a discretised formulation whereby the PSD of modal forces at frequency k, sampled at N points at time interval Δt is denoted as $\mathbf{S}_{\overline{X},k}$ ($f_k = k/(N\Delta t)$, $k = 1,\ldots,N_f$), where N_f is the frequency bin number correspondent to the Nyquist frequency of the discretised signal.

The modal force for each mode is calculated by weighting the time history of force by the mode shape. Fig. 6a shows vertical component of walking forces by each leg sampled at 200 Hz. The sum of the forces by two feet is then calculated and the static weight is removed. The resulting dynamic force is shown in Fig. 6b. The force in this example is for walking at 1.20 Hz. The modal forces for the three modes from Fig. 3 are shown in Fig. 7.

The auto (ASD) and cross (CSD) spectral density terms of the modal forces can now be determined. The CSD is a particularly relevant quantity, as it highlights the correlations between different modal forces.

Assuming now that the modal forces are wide-sense stationary processes, their PSDs can be estimated by multiplying their DFT with its complex conjugate. Fig. 8 shows an example of the calculated ASD and CSD of the modal forces. The visible spread of energy around the peaks is characteristic of the quasi-harmonic human walking nature. In addition to the shown magnitude, the CSD also contains a phase spectrum (not shown here). Thus, at each frequency band k of the spectrum a matrix $\mathbf{S}_{\overline{X},k}$ is built from the aforementioned data and substituted into Eq. (8) to obtain a $\boldsymbol{S}_{\ddot{\mathbf{y}},\boldsymbol{k}}$ PSD matrix of simulated responses.

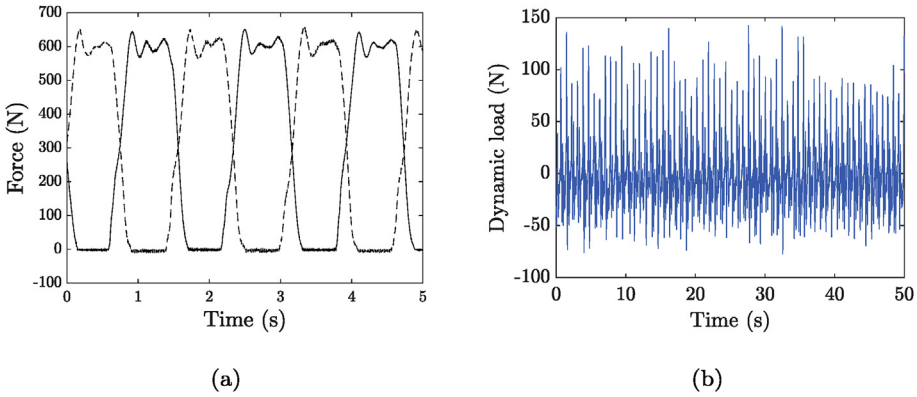

Fig. 6. Pedestrian's dynamic load recorded using an instrumented treadmill: (a) individual forces for two feet (solid and dashed lines) and (b) total force with its static component removed.

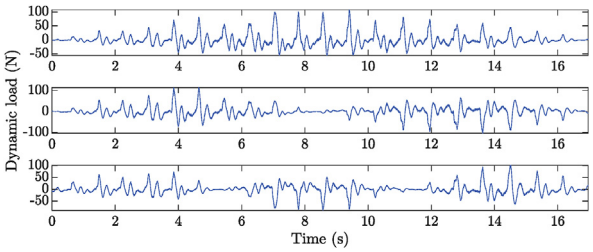

Fig. 7. Vertical modal forces for the first three vibration modes walking at 1.20 Hz.

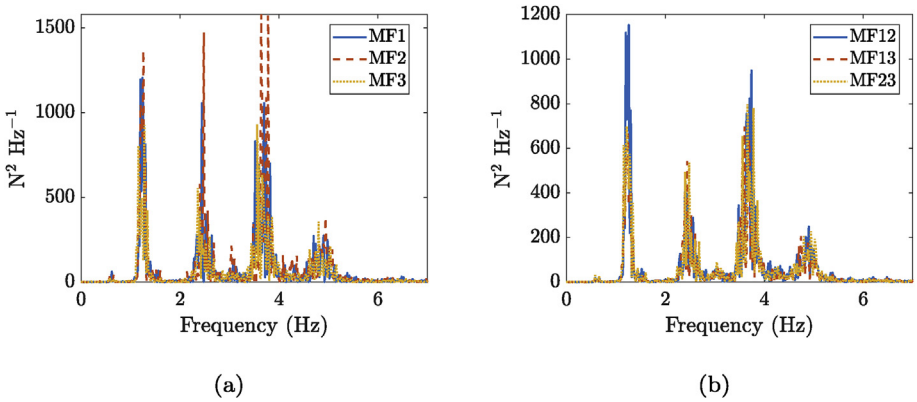

Fig. 8. (a) Auto spectral density of modal forces and (b) cross spectral density of modal force pairs. The peaks represent the 1.20 Hz pacing rate and its higher harmonics.

5. Probabilistic modal identification approach

This section details how the natural frequencies, damping ratios, and modal masses can be identified using acceleration responses.

5.1. Scaled discrete Fourier transform of observations

Let us assume that a given stochastic process, in this case the vibration response of the bridge, has N time observations $\mathbf{y}_j^e$, $j = 0, \ldots, N-1$ at N_d observation channels. The process is dependent on modal properties θ, presented in Section 2.2, as well as on the PSD of the noise at each observation channel. The scaled discrete Fourier transform (DFT) of the observations (frequency

$f_k = k/(N\Delta t))$ is given by

$$\mathbf{Y}_k = \sqrt{\frac{2\Delta t}{N}} \sum_{j=0}^{N-1} \mathbf{y}_j^e \mathrm{e}^{-\mathrm{i}2\pi jk/N} \tag{9}$$

where Δt is the sampling time interval. The scaled DFTs on a selected frequency band represent the core evidence used to identify the modal properties.

5.2. Likelihood function

The likelihood function is a joint probability density function (PDF) of a collection of variables indexed by $k\{\mathbf{Y}_k\}$ for given θ. Assuming long data, $\{\mathbf{Y}_k\}$ are (circularly symmetric) complex Gaussian and independent at different frequencies. This gives

$$p(\{\mathbf{Y}_k\}|\theta) = \prod_k p(\mathbf{Y}_k|\theta) \tag{10}$$

where the product is taken over all frequencies in the selected band with N_f DFT points, assumed to be large compared to 1 (long data); and

$$p(\mathbf{Y}_k|\theta) = \frac{\pi^{-N_d}}{|\mathbf{S}_k(\theta)|} \exp\left[-\mathbf{Y}_k^{\mathrm{H}} \mathbf{S}_k(\theta)^{-1} \mathbf{Y}_k\right] \tag{11}$$

where $\mathbf{S}_k(\theta)$ is a theoretical PSD matrix of data (Hermitian) for a given θ. The complex Gaussian probability density function (PDF) in Eq. (10) is central to the proposed modal analysis framework, as it holds for general stationary data regardless of the frequency content of contributing activities. The latter affects $\mathbf{S}_k(\theta)$ but not the form of the PDF.

Next the derivation of $\mathbf{S}_k(\theta)$ is detailed. Within a selected frequency band k, the following model is assumed

$$\mathbf{Y}_k = \hat{\mathbf{Y}}_k + \boldsymbol{\varepsilon}_k \tag{12}$$

where $\hat{\mathbf{Y}}_k$ and $\boldsymbol{\varepsilon}_k$ represent scaled DFTs of a theoretical structural dynamic response and measurement noise, respectively. Similarly, the theoretical PSD of the data is given by

$$\mathbf{S}_k(\theta) = \mathrm{E}[\hat{\mathbf{Y}}_k \hat{\mathbf{Y}}_k^{\mathrm{H}}|\theta] + \mathrm{E}[\boldsymbol{\varepsilon}_k \boldsymbol{\varepsilon}_k^{\mathrm{H}}|\theta] \tag{13}$$

assuming that the modal forces and the measurement noise are independent. $\mathrm{E}[\boldsymbol{\varepsilon}_k \boldsymbol{\varepsilon}_k^{\mathrm{H}}|\theta] = \mathrm{diag}(S_e^1, S_e^2, \ldots, S_e^{N_d})$, is a diagonal matrix, where each entry S_e^j is the PSD of noise in the frequency band (assumed as constant) at the j-th observation channel. Finally, the PSD of the structural response term can be obtained from a modal contribution form, already presented in Eq. (8), and the DFT of the structural dynamic response $\hat{\mathbf{Y}}_k$ is obtained from Eq. (7).

5.3. Log-likelihood function

Mainly for numerical reasons, it is common practice to work with the log-likelihood function (LFF) instead of the likelihood in Eq. (11), which can be expressed as

$$\mathscr{L}(\theta) = -N_d N_f \ln \pi - \sum_k \ln |\mathbf{S}_k(\theta)| - \sum_k \mathbf{Y}_k^{\mathrm{H}} \mathbf{S}_k(\theta)^{-1} \mathbf{Y}_k. \tag{14}$$

In order to identify the modal properties the LLF is sampled with the Metropolis–Hastings (MH) algorithm [18]. The samples of θ indicate in which regions of the parameter space the bridge-pedestrian model matches available data. In addition to the likelihood maximum, the samples allow to compute other uncertainties, such as the variance of the estimate.

The current section is closed with a discussion of some numerical details. In order to increase the numerical stability of the matrix inversion in Eq. (14), the matrix is transformed with a Cholesky decomposition routine. Further details of this operation are given in Appendix A.1. Relatively to the MH algorithm, it is necessary to set a proposal probability distribution (proportional to the target distribution), amongst other options which are summarised in Appendix A.2.

6. Results and discussion

6.1. Numerical tests - constant modal properties

A large number of numerical tests have been run to assess the performance of the pedestrian-based approach. Based on the results from Section 2.2, fixed modal parameters were used to generate responses to walking at 12 pacing rates (see Table 2) using MATLAB. Each force time history measured on the treadmill was weighted by the measured shape of each vibration mode (as in the RHS of Eq. (2)) to determine modal forces for each mode. The modal forces were used to calculate the modal responses

Table 2
Fixed modal parameters and pacing rates used for response generation.

f_1	f_2	f_3 (Hz)	ζ_1	ζ_2	ζ_3 (%)	m_1	m_2	m_3 (kg)
4.70	15.1	28.9	2.4	2.8	2.7	862	907	839

Pacing rates (Hz)											
1.40	1.55	1.60	1.75	1.80	1.88	2.00	2.05	2.20	2.25	2.30	2.45

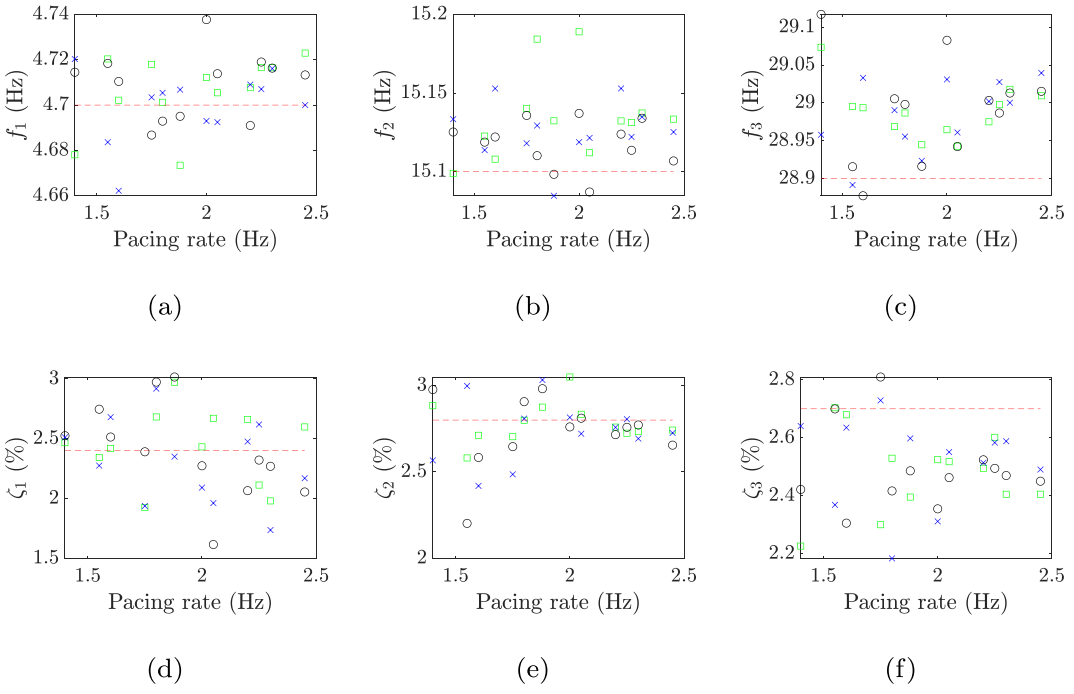

Fig. 9. Identified (a–c) natural frequencies and (d–f) damping ratios at several pacing rates for first (squares), second (crosses) and third runs (circles), and their true value (horizontal dashed line).

in each individual vibration mode using the Fox and Goodwin's numerical procedure [19]. Then, the mode superposition principle was employed to calculate the final acceleration response $\ddot{y}_i(t)$ at a location i on the deck, given by:

$$\ddot{y}_i(t) = \sum_{k=1}^{3} \phi_{i,k} \ddot{q}_k(t), \tag{15}$$

where $\phi_{i,k}$ is the amplitude of the kth mode shape ($k = 1, 2, 3$) at location $i (i = 1, \ldots, 9)$ along the midline of the bridge (crosses in Fig. 2a) and $\ddot{q}_k(t)$ is the modal response in the kth mode. Three sets were generated for each pacing rate, by dividing the available walking data into three segments, each long enough for a bridge crossing. This was done to assess the impact of the variability in the force and responses on the accuracy of the system identification.

The parameters were identified by maximising the LLF in Eq. (14) by means of the fmincon MATLAB function, rather than sampling it with the MH algorithm; mainly to avoid having to adjust the MH settings for each run. Therefore the identified values correspond to maximum likelihood estimates. It is also important to stress that a small amount of white noise ($\sigma = 1 \times 10^{-2}$ ms^{-2}) has been added to the signal, so that matrix $\mathbf{S}_{\overline{\chi}}$ in Eq. (8) remains semi-positive definite in regions of low spectral density. Not doing so in a simulated example can lead to numerical instabilities and inaccurate identifications.

The identified natural frequencies, damping ratios and modal masses are shown in Fig. 9 and Fig. 10. The modal properties are identified within a small error margin except for the first damping ratio, which ranges from 1.5% to 3.0%. The other two damping ratios are less scattered and have a smaller relative error (up to 10.7% for ζ_2 and 18.5% for ζ_3). Squares, crosses and circles in Fig. 9 and Fig. 10 represent results for the first, two and all three runs, respectively.

For the identification of modal masses, Fig. 10, the method performs well across all vibration modes, attaining the best results in the central region of pacing rates.

The relative error is shown in Table 3. Each row of the table corresponds to an error of a cumulative average of the values shown in the above plots, i.e., for one, two and all three runs across the bridge. The averages were calculated considering all pacing rates. It can be seen that the errors for natural frequencies are negligible and the largest absolute value for the error is

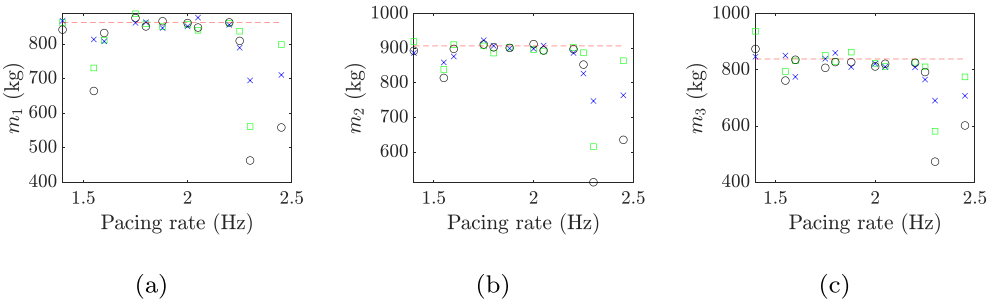

Fig. 10. Identified (a–c) modal masses at several pacing rates for first (squares), second (crosses) and third runs (circles), and their true value (horizontal dashed line).

Table 3
Relative error (%) of identifications for an increasing number of runs averages.

Averages	f_1	f_2	f_3	ζ_1	ζ_2	ζ_3	m_1	m_2	m_3
1	0.13	0.23	0.30	1.63	−0.61	−8.07	−5.66	−4.20	−3.26
2	0.06	0.20	0.30	−1.02	−1.45	−7.44	−5.26	−4.38	−3.99
3	0.10	0.17	0.30	−0.71	−1.79	−7.53	−6.76	−5.55	−5.32

Table 4
Polynomial regression coefficients of amplitude-dependent modal properties.

Parameter		α_0	α_1	α_2	α_3	α_4	α_5
f_1	Hz	4.872	−0.4958	0.3387	−0.1227	0.02112	−0.001364
ζ_1	%	2.07	1.17	−1.37	$6.79 \cdot 10^{-1}$	$-1.53 \cdot 10^{-1}$	$1.24 \cdot 10^{-2}$

about 8% for ζ_3. There is no significant error improvement beyond a single run across the bridge. This error is a consequence of treating the measured signals as wide sense stationary in Eq. (8). The error can be said to be sufficiently small for practical purposes. Note that for longer bridges this error would further decrease.

6.2. Numerical tests - amplitude-dependent modal properties

This section highlights a more challenging simulated example of modal identification with amplitude-dependent modal properties. In an attempt to emulate the real behaviour of the footbridge, the first natural frequency and damping ratio were modelled as amplitude-dependent. Specifically, they were modelled as 5th order polynomial functions of the peak acceleration (see Table 4) as obtained fitting free-decay data. The equation of motion was solved by using Fox and Goodwin's numerical procedure [19]. Since the damping ratio and natural frequency of the first mode are functions of vibration amplitude (Table 4), their values for simulating the response in the next vibration cycle are taken using maximum absolute values from the previous cycle. When simulating a response in the first cycle, the values of 4.872 Hz and 2.073% were used (free coefficients in Table 4). All the other modal parameters were kept constant, as defined in the previous section.

The identified natural frequencies are shown in Fig. 11. The shaded area in Fig. 11a shows an actual range of natural frequencies that corresponds to the vibration amplitude range. The identified natural frequency lies within the area, i.e., the method approximates the amplitude-dependent natural frequency with a constant value from within the actual range. Similarly to the previous section, the other natural frequencies are identified within a small error margin (up to 1.99% for f_2 and 1.38% for f_3).

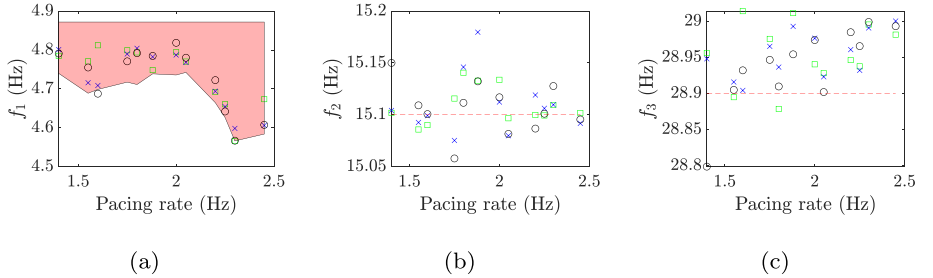

Fig. 11. Identified (a–c) natural frequencies at several pacing rates for first (squares), second (crosses) and third runs (circles) and their true values (shaded area and horizontal dashed lines).

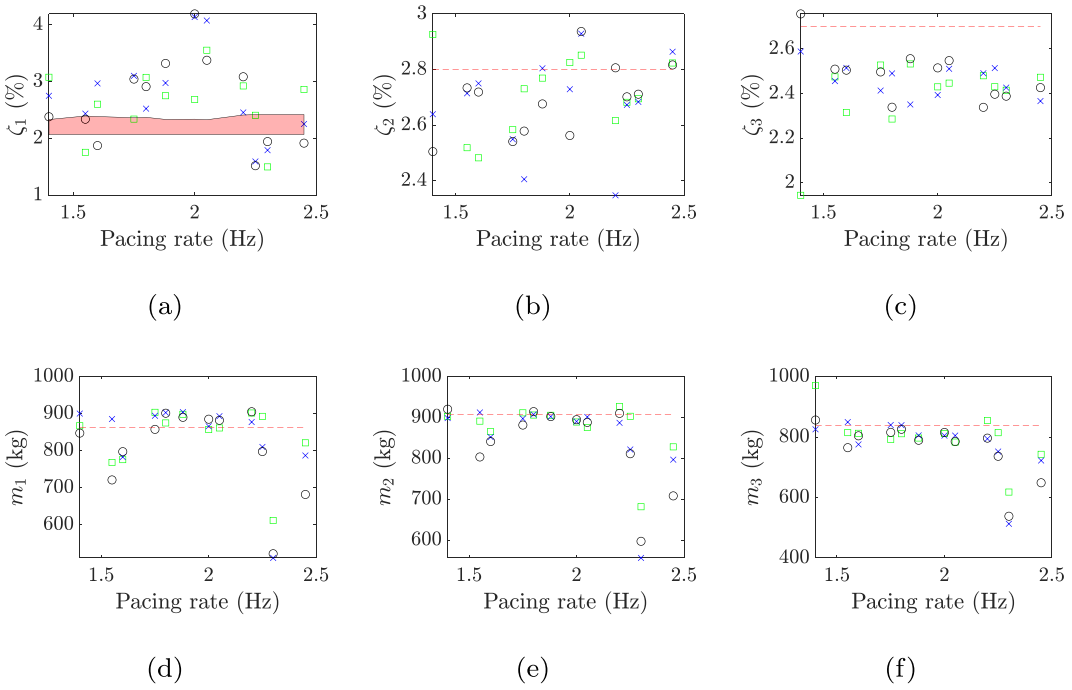

Fig. 12. Identified (a–c) damping ratios and (d–f) modal masses at several pacing rates for first (squares), second (crosses) and third runs (circles), and their true value (shaded areas and horizontal dashed lines).

Table 5
Relative error (%) of identifications for an increasing number of runs averages.

Averages	f_1	f_2	f_3	ζ_1	ζ_2	ζ_3	m_1	m_2	m_3
1	−0.82	0.06	0.19	18.16	−3.26	−11.24	−3.03	−3.67	−4.44
2	−0.96	0.06	0.18	21.04	−3.87	−10.06	−3.12	−4.88	−5.91
3	−1.00	0.05	0.17	20.55	−3.89	−9.41	−4.20	−5.75	−6.90

Fig. 12 shows the identified damping ratios and modal masses. Similarly to the previous section, modal masses are identified in a consistent manner across all three vibration modes, whereas the first damping ratio has a larger variability across pacing rates than the other two ratios. Compared with the results in the previous section the estimate of damping ratios identification have worsened, which suggests that identification of these modal properties is susceptible to nonlinear effects. For the modal masses, Fig. 12d–f indicate a reliable estimation within a central band, from 1.75 Hz to 2.20 Hz of the pacing rates, while the results are more erroneous for pacing rates at 1.55 Hz and 2.30 Hz, whose third and second harmonic, respectively, are close to the natural frequency of the first mode. In the authors' opinion, the reason is that close peaks are present in the spectrum in these tests and the identification becomes sensitive to frequency resolution of the signal, which is particularly coarse in case of faster walking (when the time domain signal is shorter).

As in the previous section, the relative error of the identifications is shown in Table 5. For the amplitude-dependent modal properties, the "true" value was considered as the mid-value of the lines that outline the shaded areas in Fig. 11 and Fig. 12a. For the current example the damping ratios have the largest observed errors, and once again, there is no considerable difference between the average error with one or more runs across the bridge.

6.3. Measurements on the footbridge

In this section acceleration data measured at TP2 and TP5 on the actual footbridge (Fig. 4) are used for validation of the pedestrian-based approach. Results will be compared against measured modal properties reported in Section 2.2.

The MH algorithm was fine-tuned to obtain the distribution of the modal properties with a burn-in period 6000 of samples, followed by a total of 10 000 samples. Since the data in Sections 2.2 and 4 were sampled at 256 Hz and 200 Hz, respectively, the former has been resampled down to 200 Hz, so that the theoretical and experimental PSD responses have the same frequency resolution. The results related to walking at 1.40 Hz, 1.55 Hz, 1.60 Hz, 1.75 Hz, 1.80 Hz, 1.88 Hz, 2.00 Hz, 2.05 Hz, 2.25 Hz, 2.30 Hz

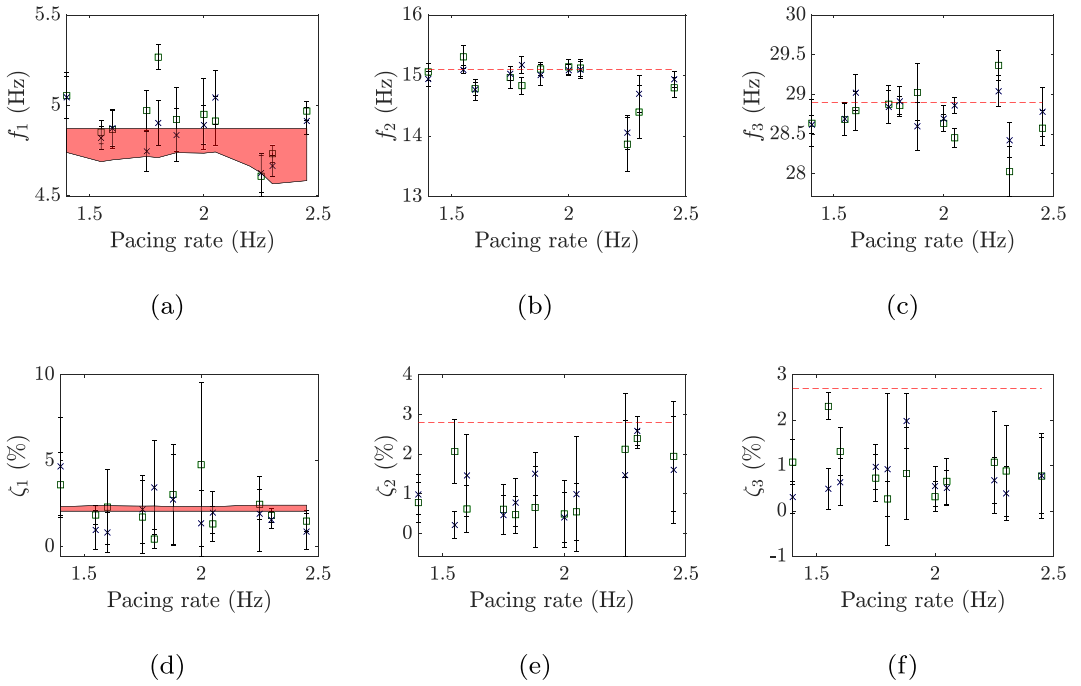

Fig. 13. Identified (a–c) natural frequencies and (d–f) damping ratios, mean values (circles) and 99.7% confidence intervals (error bars) for different pacing rates. The reference values are the shaded area and horizontal dashed lines.

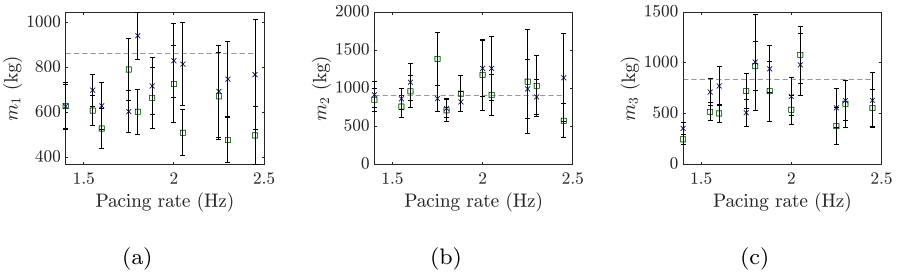

Fig. 14. Identified (a–c) modal masses mean values (circles) and 99.7% confidence intervals (error bars) at several pacing rates. Their reference values are the horizontal dashed lines.

and 2.45 Hz are presented.

One of the differences relative to the previous numerical examples is that the measured vibration response is caused by a force generated by a person walking over the bridge that inevitably differs from the treadmill force used in the analysis [20,21].

The estimated natural frequencies and damping ratios are shown in Fig. 13. The error bars represent a 99.7% confidence interval of the estimate computed from the MH samples, and the squares and crosses represent the identified mean value for the first and second run, respectively.

The identifications of the second and third damping ratio are biased because of their sensitivity to nonlinearities and the now present intra-subject variability. If the walking frequency in Fig. 8 is slightly offset from the pedestrian's step rate on the bridge, there is an offset between the harmonics of these two types of excitation, which would be increasingly larger the higher the harmonic is. Thus, higher frequencies are more affected by intra-subject variability than lower frequencies, which agrees with the presented results for the second/third and the first damping ratio, respectively.

To further minimise errors, the time lag between treadmill and in-field recordings should also be as small as possible, especially if the test subject is inexperienced with walking tests.

Lastly, the modal masses identification is shown in Fig. 14. The error has increased in comparison with the numerical examples, but it is still within 30% mark achieved when using other more elaborate test setups. The increase in this error is partially due to uncertainty of the actual modal masses associated with estimating them using the FE model.

The relative errors are presented in Table 6. The maximum absolute value of the error is up to 3%, 69% and 22% for natural

Table 6
Relative error (%) of average of identifications for field measurements.

Averages	f_1	f_2	f_3	ζ_1	ζ_2	ζ_3	m_1	m_2	m_3
1	2.94	−1.62	−0.61	−1.79	−58.61	−65.61	−29.25	3.94	−26.06
2	2.23	−1.47	−0.52	−6.28	−58.99	−68.97	−22.03	6.15	−20.97

frequencies, damping ratios and modal masses, respectively. The main difference comparatively to the numerical examples is the more pronounced bias of the identified second and third damping ratios.

The errors for natural frequencies and modal masses are sufficiently small to be competitive against other types of tests (shaker, impact hammer and ambient), whilst the errors in damping ratios can be large. Overall, simplicity in data collection using the proposed method and promising nature of the results suggest that the method has potential to be used in system identification and it is worth investigating and improving further in future research.

7. Conclusions

An approach, with potential to identify modal properties using a pedestrian excitation, has been developed and applied to a lightweight FRP footbridge. The approach was validated against both numerical and field data.

The methodology was found to provide reliable modal properties estimates, with the exception of damping ratios when considering a structure with amplitude-dependent behaviour. Generally, the best results are obtained with pacing rates that are not close to the structure's resonant frequency. Additionally, preliminary numerical tests (not presented here) indicate that the approach can be applied to heavier and less responsive bridges with similar error margins. Therefore, future work is required to explore the extents of the methodology.

The proposed model can be further developed by replacing the treadmill-based pedestrian walking forces by a probabilistic model of an overground walker; or by enhancing the proposed statistical model to account for model bias and human-structure interaction effects; and reimplementing the approach on the basis of a structure with amplitude-dependent behaviour to improve the identification of damping ratios.

Nevertheless, the reported errors for natural frequencies and modal masses are sufficiently small comparatively to the typically used tests. Thus, the pedestrian-based approach's reliability, cost-effectiveness and simplicity further justify future developments.

Author contribution statements

A.J. and S.Z. conceived the presented idea, discussed the results and contributed to the final manuscript. A.J. developed the theory and performed the computations. S.Z. provided the simulated and experimental data. A.A. verified the numerical methods developed by A.J.

Data availability

The raw and processed data required to reproduce these findings can be found at [22] for the modal tests, and [23] for the simulated and measured vibration responses, the Matlab code and the walking forces. For any other data query, please contact the corresponding author.

Acknowledgements

The authors would like to thank the anonymous reviewers/editor and Julia Dinan for feedback on the manuscript. The research in this paper was partially supported by the UK Engineering and Physical Sciences Research Council (grant number EP/M021505/1 Characterising dynamic performance of fibre reinforced polymer structures for resilience and sustainability).

Appendix A. Computational aspects

A.1. Cholesky decomposition

This section details some of the computational aspects of the proposed framework. Although matrix $S_k(\theta)$ in Eq. (11) is not expected to be very large – its dimension corresponds to the number of DOF – it can become ill-conditioned. Furthermore, determining its inverse and determinant can be computationally costly. The current approach exploits the fact that it is an Hermitian semi-positive definite matrix, and therefore, can be factorised with the Cholesky decomposition as

$$\mathbf{S}_k(\theta) = \mathbf{C}(\theta)\mathbf{C}(\theta)^{\mathrm{H}}, \tag{A.1}$$

with $\mathbf{C}(\theta)$ as a lower triangular matrix. This transformation allows an orthogonal transformation from the generalised to ordinary least squares solution of the overdetermined system to be performed:

$$\mathbf{C}_k(\theta)\widetilde{\mathbf{Y}}_k = \mathbf{Y}_k. \tag{A.2}$$

Having presented the factorisation, the original dataset $\mathbf{Y}$ and the PSD matrix of the theoretical model can now be very simply replaced by their transformed equivalents to simplify the likelihood functions shown in the original formulation. Thus, Eq. (11) becomes

$$p(\mathbf{Y}_k|\theta) = \frac{\pi^{-N_d}}{|\mathbf{C}_k(\theta)|^2} \exp[-\widetilde{\mathbf{Y}}_k^{\mathrm{H}}\widetilde{\mathbf{Y}}_k] \tag{A.3}$$

and Eq. (14) becomes

$$\ell(\theta) = -N_d N_f \ln \pi - 2\sum_k \ln |\mathbf{C}_k(\theta)| - \sum_k \widetilde{\mathbf{Y}}_k^{\mathrm{H}}\widetilde{\mathbf{Y}}_k. \tag{A.4}$$

A.2. Details of the Metropolis–Hastings algorithm

The Metropolis–Hastings algorithm belongs to the class of Markov Chain Monte Carlo (MCMC) algorithms, that approximate a target multi-dimensional probability distribution with a large number of samples. The algorithm has to be fine-tuned so that the obtained samples reflect the target distribution faithfully, i.e. regions of low probability density are visited less frequently by the sampling routine than regions of high density. In the context of the current work, each dimension of the sampled target distribution corresponds to one of the modal properties and noise PSD.

An important aspect of the whole procedure is the correlation between identified modal parameters, which has to be as low as possible. An indicator of the correlation between modal properties marginal PDFs is the correlation matrix, defined as

$$\mathbf{R}(\theta) = (\mathrm{diag}(\mathbf{\Sigma}))^{-\frac{1}{2}}\mathbf{\Sigma}(\mathrm{diag}(\mathbf{\Sigma}))^{-\frac{1}{2}}, \tag{A.5}$$

where $\mathbf{\Sigma}$ is the modal parameters covariance matrix, and $\mathrm{diag}(\mathbf{\Sigma})$ is a diagonal matrix of the elements of $\mathbf{\Sigma}$. The entries of the correlation matrix represent the Pearson coefficients, i.e. the linear dependency between the parameters, with a $-1, 0, 1$ representing a perfectly negative, lack of, or perfectly positive correlation between parameters, respectively.

Furthermore, three other options have to be set:

1. a proposal distribution that guides where the Markov chain will move at each iterative step;
2. a random generator routine for each of the sampled parameters;
3. the number of burn-in samples, to skip low probability density regions during the initial steps of the chain;

In the current work, a uniform distribution g has been adopted as the proposal distribution, within an interval $[-\delta; \delta]$ as follows

$$g(\theta'|\theta) = \begin{cases} \dfrac{1}{2\delta} & \text{for } -\delta \le \theta - \theta' \le \delta \\ 0 & \text{for } \theta - \theta' < -\delta \text{ or } \theta - \theta' > \delta \end{cases} \tag{A.6}$$

where θ and θ' correspond to a current and newly generated sample of the modal properties, respectively. The random sample generator was also assumed as a uniform sampling grid, centred at θ and within a $\pm\delta$ interval. The burn-in period was set as 2000 for a total amount of 10000 samples of a symmetric target distribution.

The factor with more influence in the correlation of the samples and convergence speed of the MH algorithm is the proposal distribution's jumping width vector, δ. The jumping width must be large enough so that the modal parameters are not excessively correlated. In a scenario when there is a trade-off between a reasonable acceptance rate and uncorrelated modal parameters, it is necessary to increase the total amount of samples and involved computational effort.

References

[1] J. Brownjohn, P. Reynolds, S.-K. Au, D. Hester, M. Bocian, Experimental modal analysis of civil structures: state of the art, in: SHMII 7th International Conference on Structural Health Monitoring of Intelligent Infrastructure, 2015.
[2] E. Caetano, Á. Cunha, Modal testing of the Vasco daGama bridge, Portugal, in: C. Boller, F.-K. Chang, Y. Fujino (Eds.), Encyclopedia of Structural Health Monitoring, John Wiley & Sons, Ltd, Chichester, UK, 2008,https://doi.org/10.1002/9780470061626.shm168.
[3] F. Magalhães, E. Caetano, . Cunha, O. Flamand, G. Grillaud, Ambient and free vibration tests of the Millau Viaduct: evaluation of alternative processing strategies, Eng. Struct. 45 (2012) 372–384.
[4] S.-K. Au, Uncertainty law in ambient modal identificationPart I: theory, Mech. Syst. Signal Process. 48 (2014) 15–33.
[5] S.-K. Au, Uncertainty law in ambient modal identificationPart II: implication and field verification, Mech. Syst. Signal Process. 48 (2014) 34–48.
[6] C.W. Kim, M. Kawatani, J. Hao, Modal parameter identification of short span bridges under a moving vehicle by means of multivariate AR model, Struct. Infrastruct. Eng. 8 (2012) 459–472.
[7] P. Reynolds, A. Pavic, Impulse hammer versus shaker excitation for the modal testing of building floors, Exp. Tech. 24 (2000) 39–44.
[8] R.R. Craig, A. Kurdila, R.R. Craig, Fundamentals of Structural Dynamics, second ed., John Wiley, Hoboken, N.J, 2006. OCLC: ocm61247316.
[9] S.-K. Au, Operational Modal Analysis, Springer Berlin Heidelberg, New York, NY, 2017.
[10] J. Brownjohn, A. Pavic, Experimental methods for estimating modal mass in footbridges using human-induced dynamic excitation, Eng. Struct. 29 (2007) 2833–2843.
[11] J.M.W. Brownjohn, M. Bocian, D. Hester, A. Quattrone, W. Hudson, D. Moore, S. Goh, M.S. Lim, Footbridge system identification using wireless inertial measurement units for force and response measurements, J. Sound Vib. 384 (2016) 339–355.
[12] G. Piccardo, F. Tubino, Equivalent spectral model and maximum dynamic response for the serviceability analysis of footbridges, Eng. Struct. 40 (2012) 445–456.
[13] K. Lievens, G. Lombaert, K. Van Nimmen, G. De Roeck, P. Van den Broeck, Robust vibration serviceability assessment of footbridges subjected to pedestrian excitation: strategy and applications, Eng. Struct. 171 (2018) 236–246.

[14] E. Shahabpoor, A. Pavic, V. Racic, Identification of walking human model using agent-based modelling, Mech. Syst. Signal Process. 103 (2018) 352–367.
[15] X. Wei, J. Russell, S. ivanovi, J. Toby Mottram, Measured dynamic properties for FRP footbridges and their critical comparison against structures made of conventional construction materials, Compos. Struct. 223 (2019) 110956.
[16] X. Wei, H.-P. Wan, J. Russell, S. ivanovi, X. He, Influence of mechanical uncertainties on dynamic responses of a full-scale all-FRP footbridge, Compos. Struct. 223 (2019) 110964.
[17] B.J. Schwarz, M.H. Richardson, Experimental modal analysis, in: Proceedings of CSI Reliability Week, 1999.
[18] I. Yildirim, Bayesian Inference: Metropolis-Hastings Sampling, Dept. of Brain and Cognitive Sciences, Univ. of Rochester, Rochester, NY, 2012.
[19] L. Fox, E.T. Goodwin, Some new methods for the numerical integration of ordinary differential equations, Math. Proc. Camb. Philos. Soc. 45 (1949) 373–388.
[20] J. Chen, J. Wang, J.M.W. Brownjohn, Power spectral-density model for pedestrian walking load, J. Struct. Eng. 145 (2019) 04018239.
[21] M. García-Diéguez, J. Zapico-Valle, Statistical modelling of spatiotemporal variability of overground walking, Mech. Syst. Signal Process. 129 (2019) 186–200.
[22] Data for Measured dynamic properties for FRP footbridges and their critical comparison against structures made of conventional construction materials. 2019 1, http://wrap.warwick.ac.uk/117039/.
[23] Data: A spectral pedestrian-based approach for modal identification. UWE, 2019 1, http://researchdata.uwe.ac.uk/529.
[24] V. Racic, J. Brownjohn, Stochastic model of near-periodic vertical loads due to humans walking, Advanced Engineering Informatics 25 (2) (2011) 259–275, https://doi.org/10.1016/j.aei.2010.07.004.